ORIGINAL

CrossMark

Hygromorphic characterization of softwood under high resolution X-ray tomography for hygrothermal simulation

Chady El Hachem [1] · Kamilia Abahri [1] · Jérôme Vicente [2] · Rachid Bennacer [1] · Rafik Belarbi [3]

Abstract

Because of their complex hygromorphic shape, microstructural study of wooden materials behavior has recently been the point of interest of researchers. The purpose of this study, in a first part, consists in characterizing by high resolution X-ray tomography the microstructural properties of spruce wood. In a second part, the subresulting geometrical parameters will be incorporated when evaluating the wooden hygrothermal transfers behavior. To do so, volume reconstructions of 3 Dimensional images (3D), obtained with a voxel size of 0.5 μm were achieved. The post-treatment of the corresponding volumes has given access to averages and standard deviations of lumens' diameters and cell walls' thicknesses. These results were performed for both early wood and latewood. Further, a segmentation approach for individualizing wood lumens was developed, which presents an important challenge in understanding localized physical properties. In this context, 3D heat and mass transfers within the real reconstructed geometries took place in order to highlight the effect of wood directions on the equivalent conductivity and moisture diffusion coefficients. Results confirm that the softwood cellular structure has a critical impact on the reliability of the studied physical parameters.

Keywords Heat and Mass Transfers · Spruce wood characterization · Thermal conductivity · Moisture diffusion coefficient · X-ray tomography · Wood fibers segmentation

1 Introduction

Upon years, wood has been widely used as building construction material in the civil engineering community. It is mainly recommended for inside use, either as panel or as insulation material due to its thermal, acoustic and environmental performances [1]. Beside its advantages, wood can present many disadvantages, being a hygroscopic material that reacts very sensibly to hygrothermal solicitations. Therefore, it is subjected to swelling or shrinkage phenomena, depending if its relative humidity increases or decreases, respectively [2]. The physical processes of transfers, the topology of vapor, liquid, and air interfaces and their interactions with the solid matrix (contact lines, detachment of vapor bubbles solid surfaces …) make the problem extremely complex. All these constraints are responsible for many damages, structural degradation, hygrothermal properties modification [3]….

The considered wood type in this study is spruce wood. This material is known by being large trees, that exist in the most temperate and boreal regions [4, 5]. Upon age, they grow by reproducing through layering. Each layer represents a cycle in which early wood grows in spring and early summer, followed later by the latewood development [6, 7] which exhibit strong heterogeneities at the microscopic scale.

In fact, spruce wood is porous media, formed by tracheids, parenchyma and pores (called lumens) that may contain variable proportions of water and mixture of vapor and dry air. It is difficult to predict accurately the transfers through the microscopic approach mainly because it is hard to reproduce numerically complex geometrical structure of the porous medium. That's why researchers have, until now, used the macroscopic models which can override this difficulty. Various approaches for predicting the heat and mass transfers through the wooden materials are available in literature [8, 9]. Other

✉ Rafik Belarbi
   rafik.belarbi@univ–lr.fr

1   LMT, ENS-Cachan, CNRS, Université Paris Saclay, 61 avenue du Président Wilson, F-94230 Cachan, France

2   IUSTI UMR 7343, CNRS, Aix-Marseille University, 5 rue Enrico Fermi, 13453 Marseille, France

3   LaSIE, UMR 7356 CNRS Université de La Rochelle, Avenue Michel Crépeau, 17042 La Rochelle cedex1, France

researches were interested in wood's performances, either by studying its mechanical behavior, or quantifying its transfer's properties [4, 8, 10–15]. Nowadays, the apparition of the non-destructive reconstruction methods allows overcoming these difficulties.

Moreover, most of the phenomena involved at the microscopic scale are at the origin of the phenomena presented on the macroscopic scale: the macroscopic behavior of wood is strongly dependent on the mechanisms acting at the levels of the material's constituents. At the same time, there are still lacks in the knowledge concerning the definition of the problem especially when considering the anatomical anisotropy of wood. In fact, just few papers of these studies concerned the microscopic scale [16–19].

At this level, early wood is characterized by cells having relatively large cavities called lumens and thin cell walls, whereas latewood contains smaller lumens and thicker cell walls [20]. Actually, the wood cells are of a characteristic size of some micrometers. It is thus necessary to deepen the research at this scale, and use a specific experimental technique, in order to distinguish all wood's components and face the morphological complexity of the problem. Most of these techniques are non-destructive. In this study, the selected method is X-ray tomography, which offers different resolutions that belay a precision of few micrometers [21, 22].

Two distinct morphological properties can be offered by early wood and latewood, which consequently leads to different transfer behaviors.

Some studies in relation with the wood's structural characterization can be found: Trtik et al. [23] treated spruce wood's microstructure, using very small specimens, for which a voxel size of 0.7 μm was obtained on the tomograph. These authors were specifically interested on the observation of the pits and the cell walls' thicknesses. For the same voxel size, Sedighi-Gilani et al. [7] analyzed the spruce wood degradation by Physisporinus vitreus and Xylaria longipes. They calculated an approximate pores' diameter for early wood and latewood, and reported their porosity values.

Despite the fact that local heat and mass transfer properties of multi-phase flows have been performed by X-ray tomography images [24, 25], a similar study has not been considered yet for spruce wood microstructure.

Actually, most of the papers that treat wooden materials don't consider any correlation between the wood microstructure and the heat and mass transfer's properties. Hence, the necessity to develop new approaches to extract more refines structural information to simulate microscopic physical phenomena.

In this context, the objective of this paper is, first to propose a reliable microtomographic characterization of spruce wood with a small voxel size of 0.5 μm to better understand the material morphology. The studied properties for early wood and latewood phases deal with the porosity, the pore and solid size distribution, the lumens' diameters as well as the cell walls' thicknesses. Also, we present an original and efficient method to segment the wood fibers. Even though the experimental microtomographic work did not concern the hygrothermal behavior of the material, the microstructure of reconstructed volumes shows big correlation with the transfer properties. In a second part, heat and mass transfers have been performed on the 3D real reconstructed geometry of wood, and equivalent transfer's properties have been calculated in the three principal directions, in order to highlight the effect of the morphological disorder on the transport phenomena.

2 Experimental procedure

The wood's transition between two cycles is identified by having latewood cells of the older cycle preceding early wood cells of the new one. This transition presents immediate leap from small to big lumens and from thick to thin cell walls [26]. In this study, the wood specimens tested correspond to either early wood phase or latewood/early wood transition.

In order to verify the repeatability of each test, six spruce wood specimens of dimensions 2x2x20 mm³ were thoroughly prepared. They were set in a 25 °C room temperature, before being scanned using the non-destructive X-ray tomography method, which allows having 3D images of a defined volume [27]. Half the samples contained a part corresponding to the latewood/early wood transition, and the rest were cut from the early wood phase. This choice was made to compare the microstructure of both wood types. The longitudinal direction of wood was along the 20 mm side. All scanned samples were without decay, knots and obvious defects.

The specimens were scanned with MicroXCT-400 tomograph at CEREGE in Aix-en-Provence, which uses the linear attenuation method. The focal-spot size of x-ray beam was 5–7 μm. Considering that wood is a weakly absorbing material, a low voltage of 80 kV and an emission current of 50 μA were selected for all the scans performed in this study. The geometrical voxel size determined by the size and number of detector elements, and by the source-object-detector distances (magnification), was fixed to 0.5 μm. The microXCT-400 is equipped with many optical lenses that lead to an additional optical magnification. In this work, a ×40 optical lens was used [28].

For a spot size larger than the voxel size, the penumbra is limiting the image quality particularly in thick body parts and degrades the spatial resolution by producing "edge unsharpness" or blur. The adapted voltage and emission courant, and the absorptivity contrast of the different features into the sample improve the resolution. To ensure that the spatial resolution is sufficient to separate cell walls structures from the wood fibers we plot for the both samples a grey level profile line along the radial direction through several fibers

(Fig. 1). This figure shows the "edge unsharpness" of the solid that will give uncertainties in the measurements on solid wall thickness and porosity estimation. Nevertheless, we observe that the resolution and the contrast are high enough to separate the different phases with a simple threshold.

3 Post-processing

After volume reconstruction phase, many post processing softwares facilitating the microscopic analysis and available in literature can be used, like ImageJ, iMorph and Avizo [29–33].

In our case, the 3D reconstruction was achieved using the software efX. For the morphological analysis work, we developed a specific module into the iMorph software, to propose an automatic wood fiber extraction [29]. This software permits the morphological characterization of porous media. Topological descriptions of both pores and solid phases can be analyzed. In addition, a very practical interaction with 3D segmented objects is available. The binarization process that consists in identifying voxels belonging to solid or void structures is obtained through a simple threshold applied to grey level distribution of voxels. This threshold can be chosen to approach the wood porosity. The incertitude in the arbitrary threshold (close to the porosity value), mainly due to the resolution limitation will impact only the voxels located at the interface between solid and void. This systematic error will have an impact on every morphological estimation (cell wall's thickness and fiber diameter). This error will mainly impact

the cell wall's thickness estimation as only few solid voxels can be located into wall structures. The granulometry analysis of the solid structures gives a mean thickness of 5-6 μm that correspond to 10–12 voxels). For the rest of this work, and specifically for the fiber individualization process, we can consider to have enough voxels to localize the solid structures. Some morphological filters have been applied on the binarized image. A closing filter (made of one dilatation and erosion morphological filter) has been applied to connect closed wall structures and remove holes. Then every small disconnected solid objects (isolated islands) have been removed to eliminate noisy solid voxels inside pore fibers (Fig. 1).

Wood microstructure is a quasi-periodic repetition of tracheids, each one formed by cell wall and a corresponding cavity (lumen). In this study, solid phases represent the cell walls, for either tracheids or other cells like parenchyma. In this context, a specific investigation was made, in order to individualize each lumen, and extract all its morphological characteristics, hence the originality of this contribution.

In fact, lumen identification is not a trivial task [34]. Most of the classical methods try to apply filters in order to close holes in the cell wall that can be due to an insufficient resolution or to the presence of parenchyma's network. Originally used to segment cellular materials such as open cells metal foams, iMorph uses maximal ball identification and a watershed method to individualize cells. This method can be generalized to identify all porous items surrounded by walls or constrictions. Applied directly to the wood fibers, over-segmented pores are obtained as represented in Fig. 2a. Starting from this segmentation, the contact surface between adjacent pores (constriction surfaces) is characterized, and the connectivity graph joining pores to pores through a given contact surface is constructed. The pores that belong to the same lumen will be joined by large surface compared to pores that belong to different lumens connected by small parenchyma's surface. The merging process consists to merging pores with large contact surface and let disconnected pores with small contact surface. Once lumens are individualized
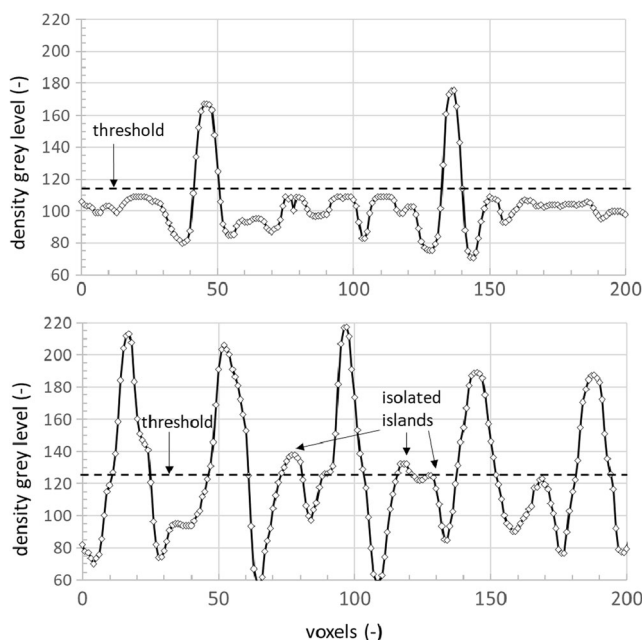

Fig. 1 Grey levels density profile line along radial directions of early (top) and latewood/early (bottom) wood for several fibers. Threshold is adjusting to fit wood porosity. Isolated islands into fibers are removed through connected components analysis
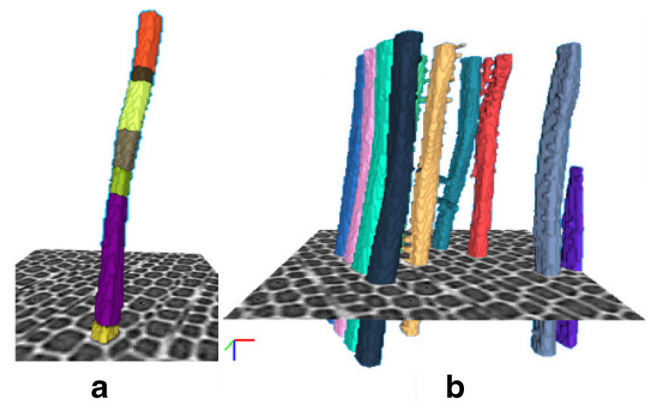

Fig. 2 Lumens' segmentation procedure: a- Over-segmented pores, b- Lumens' segmentation results

as illustrated in Fig. 2b, more precise investigation can be done to identify pits and parenchyma's network.

Firstly, the preliminary reconstructed volume contained the specimen, as well as the air around it. Therefore, a Region Of Interest (**ROI**) was cropped for each specimen to be carefully analyzed. The ROI dimensions were 600x600x1000 pixels³, which corresponds to $0.3 \times 0.3 \times 0.5$ mm³. Actually, the ROI were not necessarily oriented along the principle directions of wood. Therefore, it is important to note that for some reconstructed volumes, a rotation was performed in order to have horizontal and vertical axis respectively refer to tangential and radial directions of wood.

Secondly, pores and solid granulometries were calculated for each specimen. The corresponding results are respectively presented later on as lumens' diameters and cell walls' thicknesses distributions. Working with high resolution permits to give reliable and precise information concerning the morphological aspects of such material. Therefore, average values and standard deviations of morphological data (lumens' diameters and cell walls' thicknesses) for early wood and latewood are calculated.

4 Numerical procedure

Wood can be considered as open porous media containing variable proportion of water and a mixture of vapor and air. The nature of the resulting transfers is related to the properties of the material that can induce specific phenomena such as: evaporation/condensation, sorption/desorption and hysteresis. It is then necessary to dispose of macroscopic laws that allow us to take into account the heterogeneity and complexity of porous media and describe their overall behavior on a large scale.

One possible solution to describe the high heterogeneity on the pore scale is to assimilate it to the equivalent continuous media on a macroscopic scale, with the same average behavior, using homogenization methods, which are also called scaling method or micro–macro transition. The effective medium is then characterized by effective transport properties, or macroscopic coefficients reflecting physics at the pore scale [35]. This technique is not always valid for hygroscopic materials such wood because of their high hygromorphic character.

The proposed solution here is to simulate directly the hygrothermal behavior on the real structure of the materials. Few researches can be found on that approach; for example, Perré et al. [36] studied the spruce wood structure where 2D simulations were performed to evaluate the thermal conductivity and the moisture diffusion coefficient. The material's mechanical behavior was considered too. Indeed, the effect of the wood anisotropy on the intrinsic hygric properties has not been studied yet.

Therefore, the simulations are achieved on the real structure of a specimen of dimensions $0.3 \times 0.3 \times 0.5$ mm³, using Cast3m software [37]. The used volume represents the real 3D

structure of wood, being previously scanned by X-ray tomography. The finite element method has been used, with 8-node cubic elements.

Concerning the thermal transfer, the conventional driving potential is the temperature gradient. The energy balance equation is used where the heat transfer has been attributed to the conduction calculated by the Fourier's law, represented in equation 1 [38]. φ [W.m⁻²], λ [W.m⁻¹.K⁻¹] and T [K] correspond respectively to the heat flux, the material thermal conductivity and the temperature. Heat transfer by radiation and convection are negligible. Concerning the moisture transfer, the unanimity considers that the vapor moves inside the porous material by diffusion according to the Fick law, represented in equation 2 [39]. J [kg.m².s⁻¹], D [m².s⁻¹] and w [kg/kg] correspond respectively to the vapor flux, the moisture diffusion coefficient, and the water content. The two transfer's modes are treated separately.

$$\varphi = \lambda \, \Delta \mathrm{T} \tag{1}$$

$$\mathrm{J} = \mathrm{D} \, \Delta \mathrm{w} \tag{2}$$

The simulation task leads to extract the equivalent thermal conductivity and moisture diffusion coefficients. However, taking into consideration that the material's microstructure contains solid and air phases, the transfer properties of each phase should be attributed. After that, for each meshed element, the adapted thermal conductivity and the moisture diffusion parameters correspond to those of the element phase (solid or porosity).

Firstly, the thermal conductivity of cell walls and lumens (the air phase) should be identified for each phase. The
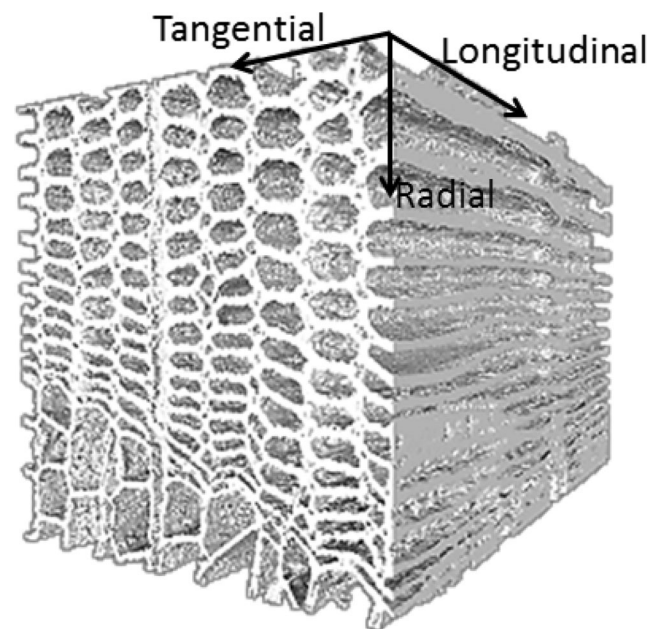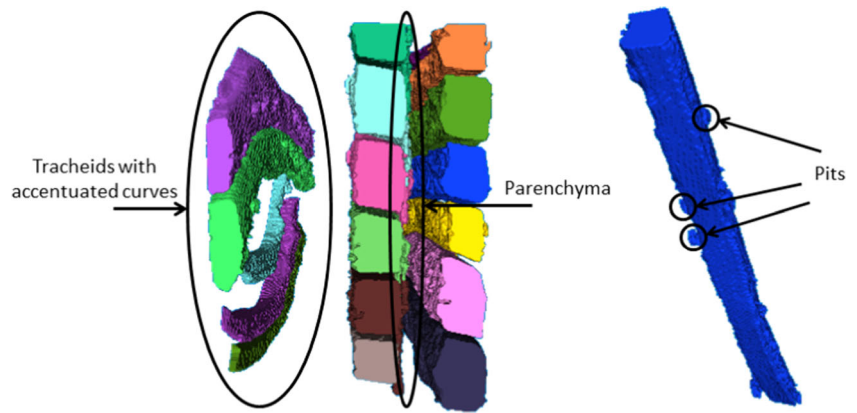

Fig. 3 Solid phase reconstruction of a ROI ($0.3 \times 0.3 \times 0.5$ mm³) of a specimen with latewood/early wood transition

Fig. 4 Individualized cavities: lumens corresponding to tracheids with accentuated curves, parenchyma and pits connecting lumens of neighbouring tracheids

thermal input parameters correspond to a conductivity factor $\lambda_{cell\ walls}/\lambda_{lumens} = 45$ [36].

By the same, the vapor diffusion coefficient was attributed for the cell walls and the lumens: the dimensionless diffusion properties are $D_{cell\ walls} = 0.004$ and $D_{lumens} = 1$ [36] for the solid and the air phases respectively. These hygric values represent bound water diffusion in wood at 12% moisture content [40] which is relatively close to the conditions of the wood specimen during the scan test. In other manner, in the hygroscopic zone, liquid-vapor interface is assumed in thermodynamic equilibrium and the liquid transfer is not considered in this zone.

The Dirichlet boundary conditions are set 1 and 0 on both sides of the solicited direction and adiabatic conditions are considered on the other sides. These conditions depend on the selected direction of the study. Finally, the equivalent macroscopic conductivity and diffusion coefficients are calculated in all 3 directions of wood (radial, tangential and longitudinal).

5 Results and discussion

In this section, various results are presented. First of all, dimensionless analysis of microstructural details of individualized

lumens is performed, which provides information about tracheids' orientation, pits and parenchyma. After that, early wood and latewood representative structural parameters are evaluated, in order to give information about lumens' diameters and cell walls' thicknesses. Finally, the reconstructed volumes served to achieve thermal and diffusion simulations in all 3 directions of wood, and the corresponding effective conductivity and diffusion coefficients are calculated, in order to highlight the anisotropy effect of such morphology on transfer properties.

5.1 Microstructural characterization

The ROI of specimens with latewood/early wood transition is presented in Fig. 3. This volume shows very refined description of the material. The latewood cell walls and their corresponding lumens are well identified, regarding their small dimensions. In addition, it is important to note that the cell walls' roughness along the longitudinal direction is easily detected.

On the other hand, some lumens present in the core of the samples are individualized (Fig. 4). Tracheids, parenchyma and pits can be easily recognized. It is known that tracheids are oriented in the longitudinal direction, parenchyma are perpendicular to the tracheids, while pits are punctuations that

Fig. 5 Lumens' diameters distribution of an early wood specimen and a specimen with latewood/early wood transition of dimensions $0.3 \times 0.3 \times 0.5$ mm^3
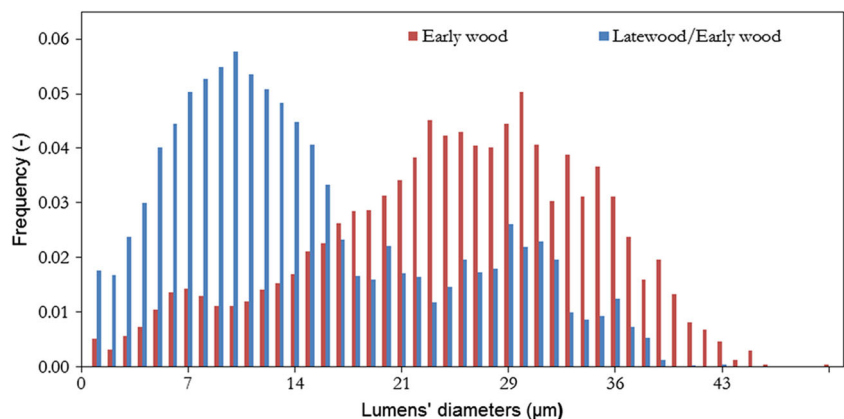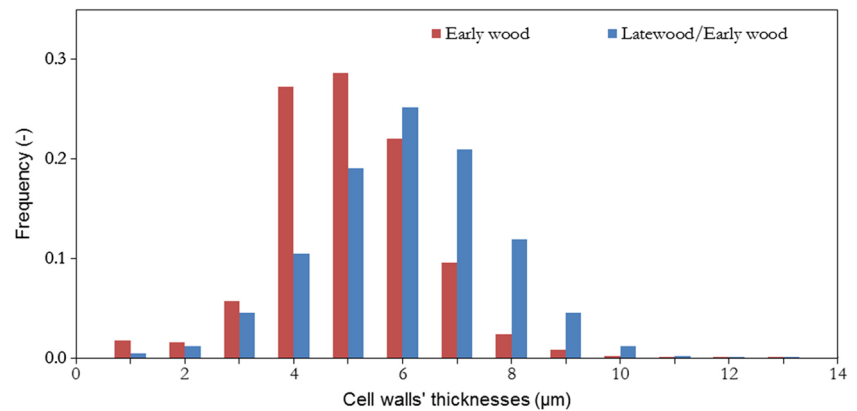
Fig. 6 Cell walls' thicknesses distribution of an early wood specimen and a specimen with latewood/early wood transition of dimensions $0.3 \times 0.3 \times 0.5$ mm^3

connect different lumens. Trtik et al. [23] showed that pits' diameters vary from 1.8 μm to 7 μm. Figure 4 shows as well that although tracheids tend to be parallel to the longitudinal direction of the tree, there could be located ones that present accentuated curves. The reason for these irregularities can be any environmental or mechanical localized solicitations, applied on a bunch of fibers, which disturb their growth and make them curve.

In order to better characterize spruce wood, cell walls' thicknesses and lumens' diameters have been calculated, for both early wood and latewood cells (Fig. 5 and Fig. 6) [41]. In fact, using a high resolution provides this work with much more diameters' variety. With such a high resolution, it is possible to calculate average and standard deviation of lumens' diameters and cell walls' thicknesses of early wood and latewood, unlike other studies that provided literature with just average values with high uncertainty, because of the limited resolution obtained. The measurements' uncertainty for both cell walls' thicknesses and lumens' diameters is calculated for a specimen scanned twice with the same environmental conditions and scan parameters, and is reported to be 0.002 for each frequency calculation.

Concerning lumens' diameters (Fig. 5), both diagrams present two distinguished peaks, the first corresponding to small cells representing latewood phase, and the second one to big cells representing early wood phase. The latewood/early wood specimen contains the most of small lumens, and the less of the biggest lumens. The biggest lumens are mainly

present in the early wood specimen. Indeed, latewood lumens have an average diameter of 11 μm, and a standard deviation of 5.5 μm, while early wood lumens have an average diameter of 27 μm and a standard deviation of 8.5 μm. Regarding literature works, Sedighi-Gilani et al. [7] obtained an approximate pores diameter of 50 μm for early wood, and reported porosity values of 79% for early wood and 27% for latewood, with a voxel size of 0.7 μm. Big similitude between these average values and the present results can be observed.

Concerning cell walls' thicknesses (Fig. 6), latewood and early wood distributions can be easily distinguished, because of the small voxel size. The average cell walls' thicknesses and their standard deviation are 6.3 μm and 1.6 μm respectively for latewood, and 5.1 μm and 1.4 μm for early wood.

The calculated parameters show different structural dimensions for early wood and latewood, as well as high standard deviations for each parameter in both wood types. Therefore, it is recommended to work with the real structure especially that it is very difficult to reproduce numerically the wood microstructure as it is, taking into consideration the parenchyma, the pits and the various irregularities that exist.

This section concerns the post-treatment of the X-ray tomography reconstructed volumes. Although this experimental work does not treat the heat and mass transfers in wood, it provides the study with qualitative interpretations. In fact, the illustrated morphological disorder, the refine identification of the pits, the parenchyma, as well as the accented anisotropy of wood, can highly influence transfers within wood. Actually,

Fig. 7 Equilibrate temperature fields calculated numerically on a volume of dimensions $150 \times 150 \times 150$ μm^3 in all directions: a- radial, b- tangential, c- longitudinal

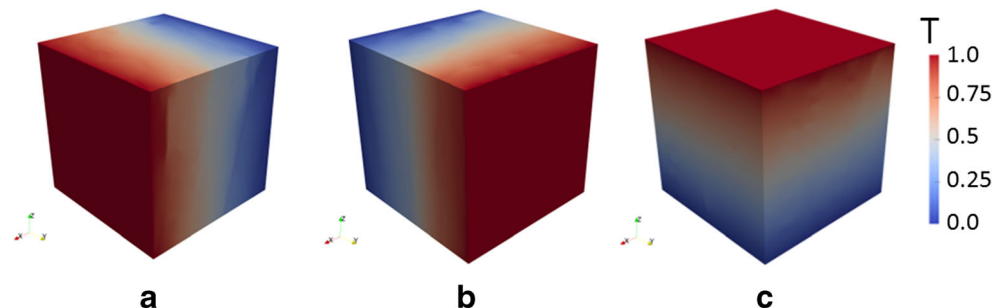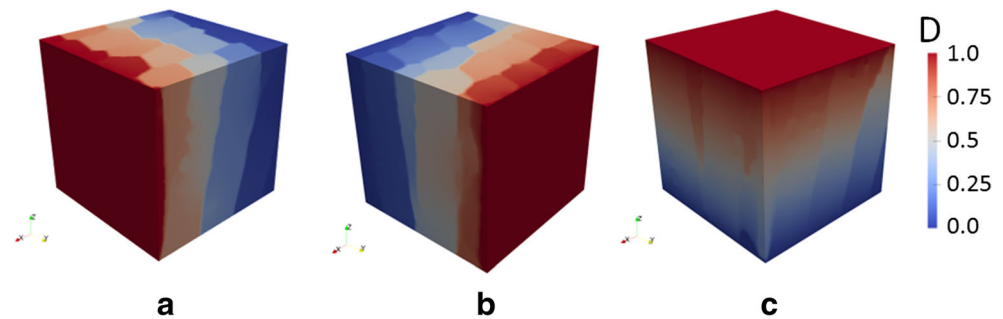**Fig. 8** Equilibrate vapor content fields calculated numerically on a volume of dimensions 150x150x150 μm^3 in all directions: a- radial, b- tangential, c- longitudinal

heat and mass transfers are affected by the morphology of the porous matrix. Hence, the elongated tracheids along the longitudinal direction and the different alignments of the cells between the radial and tangential directions influence surely the conductivity and diffusion coefficients.

The results obtained in this section serve as well as input parameters by providing further works with morphological dimensions of several spruce woods' components to simulate microscopic physical phenomena.

5.2 Hygrothermal simulation

In a first step, the temperature and vapor transfer's profiles resulting from the numerical simulation were examined. Figures 7 and Fig. 8 respectively show the temperature and the vapor content fields of a specimen of dimensions 150x150x150 μm^3, solicited in the 3 principal directions (radial, tangential and longitudinal). The corresponding equivalent thermal conductivity and moisture diffusion coefficients are shown in Table 1.

With such a small voxel size, it is difficult to make heat and mass transfer simulations within bigger volumes. However, the volume studied is sufficient to conduct a reliable study for the calculation of equivalent parameters.

Concerning heat transfer within the material, the obtained equivalent thermal conductivity is higher in the longitudinal direction, compared to the other two directions. This is due to the regular alignment of the tracheids along the axis of the tree, especially that the solid phase presents a higher conductivity than the air. Comparing the different temperature fields in Fig. 7, we can still see some inhomogeneous fields, because of the irregularities in wood.

Concerning mass transfer, the vapor content distribution is more heterogeneous; it can be distinguished on the wood cells, especially in the radial and tangential directions (Fig. 8). Visibly, these cells have a curtail role on the moisture transfer. In fact, the longitudinal equivalent diffusion coefficient shows a much higher value than the radial and tangential ones. This is certainly due to the open cavities (lumens) of the tracheids in the axis of the tree, and evidently on the high diffusivity factor between air and cell walls. On the other hand, the diffusion in the radial and tangential directions is highly dependent on the pits present in the cell walls that connect tracheids.

Actually, the heat transfer is faster in the cell walls than in the lumens, but obviously the conductivity factor is much smaller than the diffusivity regarding the insulation character of spruce wood. Therefore, for mass transfers, the diffusion fields does not show a transition phase similar to the temperature fields, because of the cell walls that brake the transfer's kinetic.

6 Conclusion

Through this study, we have shown the utility of the use of tomographic volumes for the morphological characterization of spruce wood, but also for the calculation of its hygrothermal properties under 3D real simulations.

At first, microstructural characterization was performed, and various parameters were calculated with a small voxel size of 0.5 μm. The studied properties of early wood and latewood phases deal with the porosity, the pore and solid size distribution, the average and standard deviations of lumens' diameters as well as cell walls' thicknesses. Post-processing the reconstructed volumes on iMorph served as well to develop a new technique to individualize lumens, and identify wood's pits and parenchyma.

Results reveal that early wood and latewood cells have average lumens' diameters of around 27 μm and 11 μm respectively, and average walls' thicknesses of around 5.1 μm and 6.3 μm respectively. In addition, the standard deviations calculated are considerable, and require to be taken into consideration for simulations. Obviously, both wood types' differences, which cause the anisotropy of this material, have a

Table 1 Equivalent dimensionless conductivity and diffusion coefficients in the three principal wood directions, calculated numerically on a volume of dimensions 150x150x150 μm^3

	Conductivity	Diffusion
Radial direction	0.112	0.179
Tangential direction	0.099	0.262
Longitudinal direction	0.188	0.761

considerable influence on the transfers' phenomena as well as on the mechanical properties of spruce wood.

In fact, the 3D numerical calculations realized on the real wood structure demonstrate the anisotropy effect of the equivalent hygrothermal properties: thermal conductivity and moisture diffusion coefficients. It is essentially dependent on the cells' roughness and the presence of pits within material. This anisotropy is more significant concerning the thermal conductivity which can be explained by the thermal insulation aspect of the wood. Further works, considering the swelling phenomena when studying the moisture transfer are required. In addition, further comparison of the equivalent hygrothermal parameters obtained with experimental results should be investigated.

This study provides future researches with sufficient refined structural properties concerning spruce wood's microscopic characterization. These results are primordial for either transfers or mechanical wood studies, and serve as well as input parameters for physical simulations.

References

1. Lagüela S, Bison P, Peron F, Romagnoni P (2015) Thermal conductivity measurements on wood materials with transient plane source technique. Thermochim Acta 600:45–51

2. Ranfsanjani A, Lanvermann C, Niemz P, Carmeliet J, Derome D (2013) Multiscale analysis of free swelling of Norway spruce. Composites Part A 54:70–78

3. Hervé V, Mothe F, Freyburger C, Gelhaye E, Frey-Klett P (2014) Density mapping of decaying wood using X-ray computed tomography. Int Biodeterior Biodegrad 86:358–363

4. Krause C, Déry Bouchard CA, Plourde PY, Mailly D (2013) Compression wood and stem horizontal displacement in black spruce and Jack pine plantations in the boreal forest. For Ecol Manag 302:154–162

5. Peltoniemi M, Penttilä R, Mäkipää R (2013) Temporal variation of polypore diversity based on modelled dead wood dynamics in managed and natural Norway spruce forests. For Ecol Manag 310:523–530

6. Mäkinen H, Jaakkola T, Piispanen R, Saranpää P (2007) Predicting wood and tracheid properties of Norway spruce. For Ecol Manag 241:175–188

7. Sedighi-Gilani M, Boone MS, Mader K, Schwarze FWMR (2014) Synchrotron X-ray micro-tomography imaging and analysis of wood degraded by Physisporinus vitreus and Xylaria longipes. J Struct Biol 187:149–157

8. Abahri K, Belarbi R, Trabelsi A (2011) Contribution to analytical and numerical study of combined heat and moisture transfers in porous building materials. Build Environ 46:1354–1360

9. Ferroukhi Y, Abahri K, Belarbi R, Limam K, Nouviare A (2016) Experimental validation of coupled heat, air and moisture transfer modeling in multilayer building components. Heat and Mass Transfer Journal 52:2257–2269. https://doi.org/10.1007/s00231-015-1740-y

10. Zhou Y, Fushitani M, Sato K, Ozawa M (2000) Bending creep behavior of hot-pressed wood under cyclic moisture change conditions. J Wood Sci 46:423–430

11. Virta J, Koponen S, Absetz I (2006) Measurement of swelling stresses in spruce (Picea abies) samples. Build Environ 41:1014–1018

12. Anshari B, Guan ZW, Kitamori A, Kung A, Jung K, Hassel I, Komatsu K (2011) Mechanical and moisture-dependent swelling properties of compressed Japanese cedar. Constr Build Mater 25:1718–1725

13. Murata K, Nagai H, Nakano T (2011) Estimation of width of fracture process zone in spruce wood by radial tensile test. Mech Mater 43:389–396

14. Sedighi-Gilani M, Griffa M, Mannes D, Lehmann E, Carmeliet J, Derome D (2012) Visualization and quantification of liquid water transport in softwood by means of neutron radiography. Int J Heat Mass Transf 55:6211–6221

15. Witomski P, Krajewski A, Kozakiewicz P (2014) Selected mechanical properties of Scots pine wood from antique churches of Central Poland. Eur J Wood Wood Prod 72:293–296

16. Gindl W, Schöberl T (2004) The significance of the elastic modulus of wood cell walls obtained from nanoindentation measurements. Composites Part A 35:1345–1349

17. Forsberg F, Sjödahl M, Mooser R, Hack E, Wyss P (2010) Full Three-Dimensional Strain Measurements on Wood Exposed to Three-Point Bending: Analysis by Use of Digital Volume Correlation Applied to Synchrotron Radiation Micro-Computed Tomography Image Data. Strain 46:47–60

18. Li W, Van den Bulcke J, De Windt I, Loo DV, Dierick M, Brabant L, Acker JV (2013) Combining electrical resistance and 3-D X-ray computed tomography for moisture distribution measurements in wood products exposed in dynamic moisture conditions. Build Environ 67:250–259

19. Li W, Van den Bulcke J, Mannes D, Lehmann E, De Windt I, Dierick M, Van Acker J (2014) Impact of internal structure on water-resistance of plywood studied using neutron radiography and X-ray tomography. Constr Build Mater 73:171–179

20. Trechsel HR (2001) Moisture Analysis and Condensation Control in Building Envelopes. ISBN 9780803120891, ASTM International

21. Bouterf A, Roux S, Hild F, Adrien J, Maire E, Meille S (2014) Digital Volume Correlation Applied to X-ray Tomography Images from Spherical Indentation Tests on Lightweight Gypsum. Strain 50:444–453

22. Netterer F (1986) The Mathematics of Computerized Tomography. SIAM

23. Trtik P, Dual J, Keunecke D, Mannes D, Niemz P, Stähli P, Kaestner A, Groso A, Stampanoni M (2007) 3D imaging of microstructure of spruce wood. J Struct Biol 159:46–55

24. Gulati S, Behling M, Munshi P, Luke A, Mewes D (2010) Tomographic KT-1 signature of phase-fraction distributions in multiphase bubble columns. Flow Meas Instrum 21:249–254

25. Shakya S, Munshi P, Luke A, Mewes D (2015) Computerized tomography application in oil industry using KT-2 signature. Res Nondestruct Eval 26:61–89

26. Guo J, Song K, Salmén L, Yin Y (2015) Changes of wood cell walls in response to hygro-mechanical steam treatment. Carbohydr Polym 115:207–214

27. El Hachem C, Ye P, Abahri K, Bennacer R (2017) Fiber's hygromorphic effect on thermal conductivity of wooden fibrous insulation characterized by X-ray tomography. Constr Build Mater 150:758–765

28. Bossa N, Chaurand P, Vicente J, Borschneck D, Levard C, Aguerre-Chariol O, Rose J (2015) Micro- and nano-X-ray computed-

tomography: A step forward in the characterization of the pore network of a leached cement paste. Cem Concr Res 67:138–147

29. Brun E, Vicente J, Topin F, Occelli R, Clifton MJ (2009) Microstructure and Transport Properties of Cellular Materials: Representative Volume Element. Adv Eng Mater 10:805–810

30. Schneider CA, Rasband WS, Eliceiri KW (2012) NIH Image to ImageJ: 25 years of image analysis. Nat Methods 9:671–675

31. Bird MB, Butler SL, Hawkes CD, Kotzer T (2014) Numerical modeling of fluid and electrical currents through geometries based on synchrotron X-ray tomographic images of reservoir rocks using Aviro and COMSOL. Comput Geosci 73:6–16

32. Ćosić K, Korat L, Ducman V, Netinger I (2015) Influence of aggregate type and size on properties of pervious concrete. Constr Build Mater 78:69–76

33. Levin ZS, Ted Hartwig K (2015) Hardness and microstructure of tungsten heavy alloy subjected to severe plastic deformation and post-processing heat treatment. Mater Sci Eng A 635:94–101

34. Wernersson E, Brun A, Luengo Hendriks C (2009) Segmentation of Wood Fibres in 3D CT Images Using Graph Cuts. Image Anal Process - ICIAP 5716:92–102

35. Bennai F, Abahri K, Belarbi R, Tahakourt A (2016) Periodic homogenization for heat, air, and moisture transfer of porous building materials. Numerical Heat Transfer, Part B: Fundamentals 70: 420–440

36. Perré P, Alemeida G, Ayouz M, Frank X (2016) New modelling approaches to predict wood properties from its cellular structure : image-based representation and meshless methods. Ann For Sci 73: 147–162

37. Cast3m (2016) http://www-cast3m.cea.fr/

38. Bailyn M (1994) A Survey of Thermodynamics. American Institute of Physics, New York

39. Crank J (1979) The mathematics of diffusion, 2nd edn. Clarendon Press, Oxford

40. Siau JF (1984) Transport processes in wood. Springer, New York

41. Vicente J, Wyart Y, Moulin P (2013) Characterization (2D-3D) of ceramic microfiltration membrane by synchrotron radiation: new and abraded membranes. J Porous Media 16:537–545